Geomechanics and Engineering, *Vol. 24, No. 3 (2021) 253-266*
DOI: https://doi.org/10.12989/gae.2021.24.3.253

Designing an innovative support system in loess tunnel

Zhichao Wang[1a], Yuan Xie[2,4b], Jinxing Lai[*1], Yongli Xie[1c], Xulin Su[1d], Yufeng Shi[1e] and Chunxia Guo[3f]

[1]*School of Highway, Chang'an University, Xi'an 710064, China*
[2]*Powerchina Xibei Engineering Corporation Limited, Xi'an 710065, China*
[3]*School of Science, Xi'an University of Architecture and Technology, Xi'an 710055, China*
[4]*Institute of Geotechnical Engineering, Xi' an University of Technology, Xi'an 710048, China*

(Received March 13, 2020, Revised January 18, 2021, Accepted January 21, 2021)

Abstract. The sufficient early strength of primary support is crucial for stabilizing the surroundings, especially for the tunnels constructed in soil. This paper introduces the Steel-Concrete Composite Support System (SCCS), a new support with high bearing capacity and flexible, rapid construction. The bearing characteristics and construction performance of SCCS were systematically studied using a three-dimensional numerical model. A sensitivity analysis was also performed. It was found that the stress of a π-shaped steel arch decreased with an increase in the thickness of the wall, and increased linearly with an increase in the rate of stress release. In the horizontal direction of the arch section, the nodal stresses of the crown and the shoulder gradually increased in longitudinally, and in the vertical direction, the nodal stresses gradually decreased from top to bottom. The stress distribution at the waist, however, was opposite to that at the crown and the shoulder. By analyzing the stress of the arch section under different installation gaps, the sectional stress evolution was found to have a step-growth trend at the crown and shoulder. The stress evolution at the waist is more likely to have a two-stage growth trend: a slow growth stage and a fast growth stage. The maximum tensile and compressive stresses of the secondary lining supported by SCCS were reduced on average by 38.0% and 49.0%, respectively, compared with the traditional support. The findings can provide a reference for the supporting technology in tunnels driven in loess.

Keywords: loess tunnel; steel-concrete composite support system; tunneling; mechanical property; stress distribution

1. Introduction

Steel arch and shotcrete provide a common form of initial support structures for tunnels (Bonini *et al.* 2013, Dancygier *et al.* 2016, Kaya *et al.* 2017, Rahimi *et al.* 2014, Rehman *et al.* 2018, Yoo and Choi 2018). This technology, however, makes it difficult to achieve the desired bearing capacity and close the support to form the ring structure rapidly in some cases (Bjureland *et al.* 2017, Doostmohammadi, 2016, Wang *et al.* 2019a, Wu *et al.* 2021, Xue *et al.* 2019). In addition, the quality of construction cannot be easily controlled, bolt connection between steel arches is challenging, and adhesion between shotcrete and steel arches is limited. In loess strata, in particular, the surroundings deform rapidly after tunnel excavation, and the capacity of conventional initial support appears limited (Lai *et al.* 2017, Liu *et al.* 2017, 2021, Zhang *et al.* 2019a). Excessive deformation induces the cracking of shotcrete and the distortion of the steel arch (Liu and Lai, 2019, Song *et al.* 2019, Wu *et al.* 2020, Zhu *et al.* 2019), both of which can lead to structural damage and even collapse (Fig. 1). Therefore, limiting the deformation as early as possible and avoiding ground failure is crucial for construction safety (Prazeres *et al.* 2012, Skrzypkowski *et al.* 2019, Wang *et al.* 2021a, b, c). Some research has been done on strengthening the support of loess tunnels (Li *et al.* 2020, Mao *et al.* 2019, Zhang *et al.* 2019b, Zhang *et al.* 2021c, Zhou *et al.* 2020). However, these studies were aimed at auxiliary reinforcement measures, which resulted in increased construction costs and time, while not significantly strengthening steel arch and shotcrete. This study presents a construction method that improves the bearing capacity of the traditional support for tunnels driven in loess

Concrete-filled steel tubes (CFST) typically have a high bearing capacity and low cost (Al Zand *et al.* 2016, Hassanein *et al.* 2018) and have been widely recognized and installed in underground structures (Khan *et al.* 1996, Ozdogan *et al.* 2018, Wang *et al.* 2021d). Huang *et al.* (2018) developed a new reinforced support structure, named CFST support structure, to address the long-term large-scale deformation of the deep roadway. Chang *et al.* (2014) used numerical analysis to study the load-displacement response

∗Corresponding author, Professor
E-mail: laijinxing@chd.edu.cn
[a]Engineer, Ph.D.
E-mail: wangzc@chd.edu.cn
[b]Engineer
E-mail: xieyuan@chd.edu.cn
[c]Professor
E-mail: xieyl@263.net
[d]Ph.D. Student
E-mail: suxulin@chd.edu.cn
[e]Ph.D. Student
E-mail: shiyf96@chd.edu.cn
[f]Professor
E-mail: guochunxia@xauat.edu.cn

ISSN: 2005-307X (Print), 2092-6219 (Online)

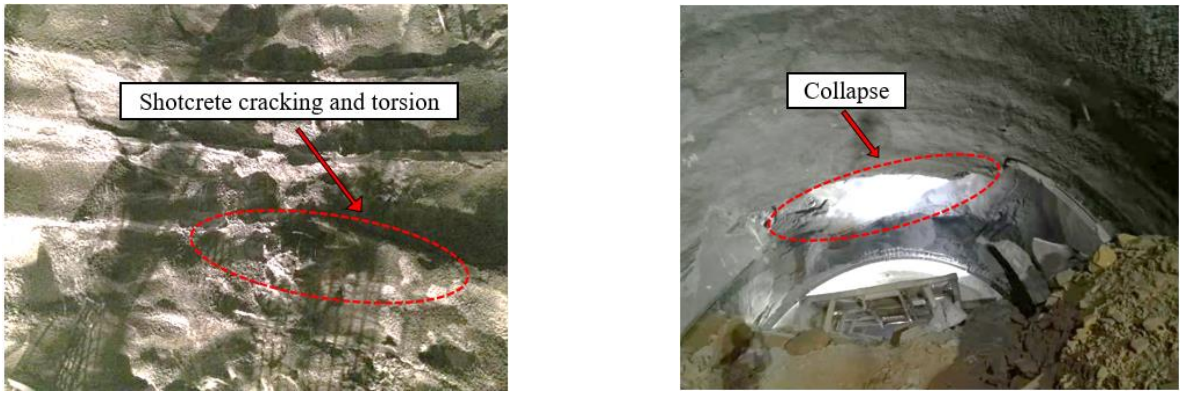

Fig. 1 Typical failure and damage in loess tunnel

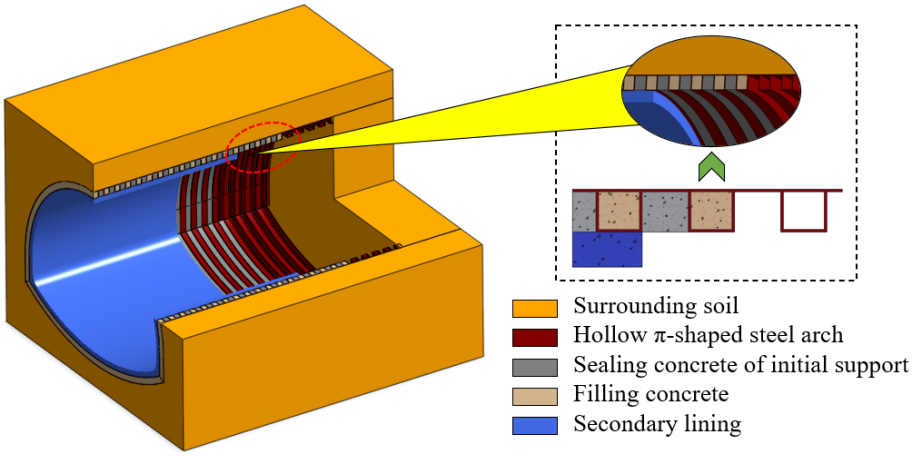

Fig. 2 Steel-concrete composite support system

of CFST under high-ground stress and divided it into three stages: elastic, elastic-plastic, and plastic. Zhang *et al.* (2017) clarified the definition and expression of the bearing capacity of the CFST arch through laboratory tests and analytical calculations. Wang *et al.* (2017) proposed a new concrete-filled square steel tube arch support system given the complex geological conditions, such as high buried depth, high stress, and structural fracture zones. Li *et al.* (2018 and 2020) put forward two typical failure modes of a casing joint by establishing a simplified calculation model of the joint, deducing its failure criteria, and establishing a method of calculating its bearing capacity. Large-section tunnel construction presents many challenges, such as weak surroundings control, low construction efficiency, and poor safety (He *et al.* 2021; Liu *et al.* 2020b). To address these challenges, Wang *et al.* (2019b) proposed a new mechanized construction technology of fabricated arches. Compared with the traditional steel arch, the strength of this arch was increased by 2.05 times.

Although the high-strength CFST support has been widely used, research on its application in tunnels constructed in loess is scarce. Also, the mechanical performance of CFST has not been studied for large-scale tunnels with sequential excavation.

In this paper, a new Steel-Concrete Composite Support System (SCCS) is proposed, which actively adapts to ground load increase and has higher bearing capacity in an early stage of construction due to a favorable stiffness ratio between primary and secondary lining. Parameters affecting the bearing capacity of SCCS were studied using a three-dimensional numerical model with the commercial software ANSYS 19.0. A sensitivity analysis was performed, including the structural stress development and the section stress distribution of the new type arch, respectively.

2. Steel-concrete composite support system

2.1 Basic composition

The main bearing body of the Steel-Concrete Composite Support System (SCCS) is the primary support that can provide high capacity in the early stages of tunnel excavation, by reducing the ground load, as shown in Fig. 2. The initial support system is composed of a steel-concrete composite arch (hereafter referred to as a π-shaped steel arch due to its shape resembling a π) and sealing concrete. The system is composed of three bearing layers:

(1) A π-shaped steel arch bearing layer. The hollow arch frame is used to close the cavity immediately and provide initial support to bear the surrounding ground load caused by the tunnel excavation.

(2) A reinforcement framework bearing layer. By injecting concrete into a tube, the hollow arch frame is filled, forming a CFST skeleton structure that can bear the increasing load of the surrounding soil.

(3) An internal filling bearing layer. The space between the steel frames is filled with sealing concrete to complete the primary lining system.

2.2 Design concepts and characteristics

Compared with the conventional support system with shotcrete and rockbolts, the SCCS has the following advantages:

(1) Increased support stiffness and bearing capacity. On the one hand, the steel-concrete composite structure has stronger compression, torsion, and bending resistance. On the other hand, sealing concrete can achieve greater thickness than shotcrete, thus overcoming the issues of hanging steel mats and large shotcrete rebounds.

(2) Higher stiffness ratio of the initial support, which is the main bearing body of the tunnels constructed in loess. Increased strength and early bearing capacity of the initial support can reduce further stress release of the surroundings in loess tunnels.

(3) A timely bearing capacity. Based on the rapid closure of the excavated cavity with a π-shaped steel arch, the concrete in the pipe and the mold is used to adapt to the gradual increase of the ground pressure in the tunnels constructed in loess.

(4) Improved stability of the arch structure. Compared with the traditional steel arch, the out-of-plane stability of the SCCS arch is significantly improved.

(5) Improved construction efficiency. The time for grouting concrete in a steel tube and the construction time for sealing concrete in the initial support can be adjusted flexibly based on the actual construction conditions and the surrounding soil deformation.

(6) The surface of the initial support is flat, making it convenient to lay the waterproof layer and improve the overall waterproof effect.

(7) Improved construction environment in the tunnel. The use of sealing concrete instead of shotcrete in construction can reduce pollution in the tunnel environment.

2.3 Construction technology

The basic construction technology of SCCS mainly includes the following points. (1) Installation of π-shaped steel arch. (2) Grouting in hollow π-shaped steel arch. (3) Filling initial support concrete. (4) Laying waterproof board. (5) Construction of secondary lining.

3. Numerical simulation

The installation of a hollow π-shaped steel arch is the first step of the SCCS. Its safety and stability are vital for the subsequent construction. Therefore, it is necessary to understand the mechanical response of a π-shaped steel arch in the process of excavation and support.

3.1 Numerical model and parameters

Construction data was gathered from the Ningxian tunnel in Qingyang, China. The V-lining section of the tunnel was selected as the research object (Fig. 3), and a numerical model was established, as shown in Fig. 4. The horizontal length of the calculation domain of the model was three times tunnel diameters (3D), the distance of the bottom boundary of the model from the tunnel invert was four times tunnel diameters (4D), and the longitudinal length was taken as 20 round lengths.

The lithology of the formation is Q_3^{eol} Malan loess and Q_2^{eol} Lishi loess (Liu 1997, Hua 2018), with a thickness of 10 m and 56 m, respectively. The surrounding soil and concrete layer were simulated by SOILD45 element embedded in ANSYS software, which has been widely used in three-dimensional solid structure. The π-shaped steel arch was simulated by BEAM188 element embedded in ANSYS software, which is based on Timoshenko beam theory and widely used in three-dimensional beam structure.

Considering the principle of overlapping grouting range (Wang 2019), the diffusion radius is taken as follows.

$$R = (0.6 - 0.7)S \quad (1)$$

where S represents the center distance of the advanced small pipe.

Based on the insertion depth and grouting diffusion radius of the advanced small pipe, the reinforcement area was determined to be 1 m. The grounting area was simulated by the strengh enhanced solid element, increasing the cohesion and internal friction angle to form the surroundings reinforcement (Chen *et al.* 2020, Liu *et al.* 2020a).The support structure was modelled as an elastic material, while the soil was modelled as an elastic-plastic material, which meets the Drucker-Prager yield criterion. A few parameters, such as density, elastic modulus, Poisson's ratio, cohesion, and internal friction angle were obtained by tests, field investigations and current Chinese tunnel standard (JTG 3370.1-2018), as shown in Table 1.

The round length was 0.7 m of per excavation cycle, and no installation gap was present between the π-shaped steel arch and the soil. According to the Technical Code for Concrete Filled Steel Tubular Structures (GB 50936-2014, 2014), the wall thickness of a steel pipe cannot be less than 3 mm. Given the economic, safety, fabrication, welding, installation, and construction factors, the wall thicknesses to be analyzed was chosen to be 4 mm, 5 mm, and 6 mm, respectively.

3.2 Stress release rate and boundary conditions

The stress release method was used to simulate a

Table 1 Calculation parameters of the model

Name	Density [kg/m^3]	Elastic modulus [MPa]	Poisson's ratio	Cohesion [kPa]	Internal friction angle [°]
Q_3^{eol} Malan loess	1450	80	0.33	15.55	28.05
Q_2^{eol} Lishi loess	1750	80	0.33	20.90	29.75
Advanced reinforcement	1750	80	0.30	25.08	35.70
π-shaped steel arch	7700	210000	0.30	-	-
Concrete	2300	31000	0.20	-	-

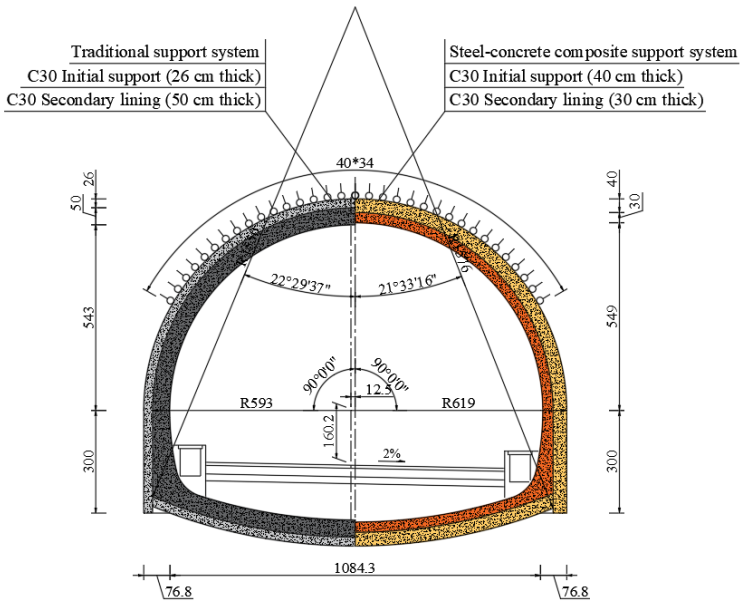

Fig. 3 Lining structure (unit: cm)

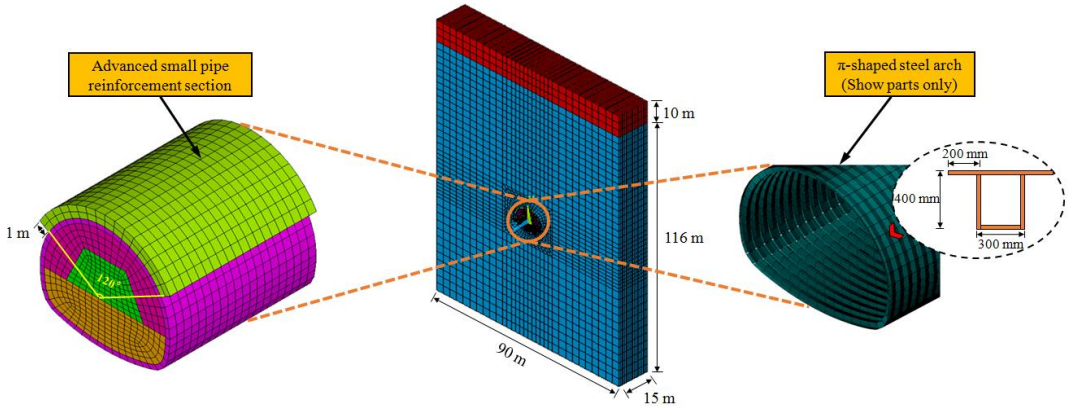

Fig. 4 Grid partition schematic diagram

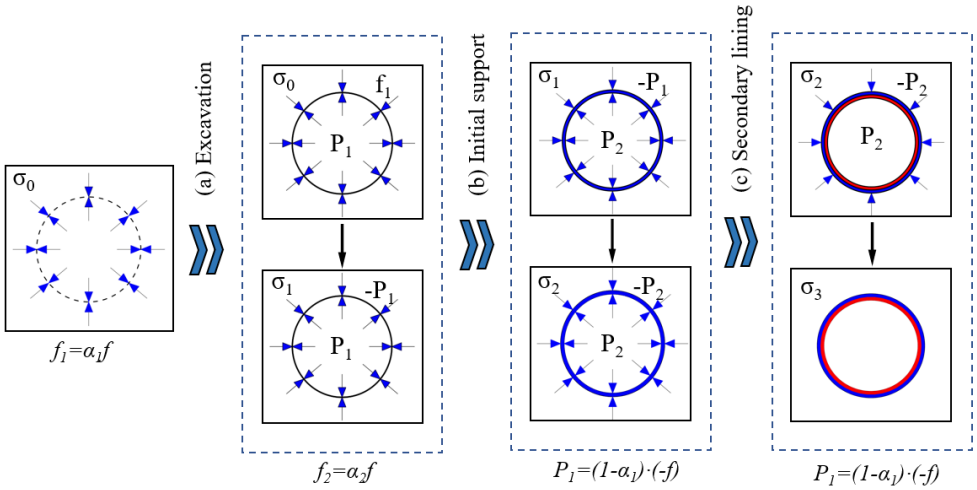

α_1 — Stress release rate of surrounding rock in different stages
α_2 — Stress release rate of surrounding rock in different stages
f_1 — Release load of surrounding rock
f_2 — Stress release of surrounding rock after initial support installation
P_1 — Fictitious support pressure
P_2 — Fictitious support pressure
σ_0 — Initial stress
σ_1 — Stress of surrounding rock
σ_2 — Stress of surrounding rock
σ_3 — Stress of surrounding rock

Fig. 5 Stress evolution process of surroundings

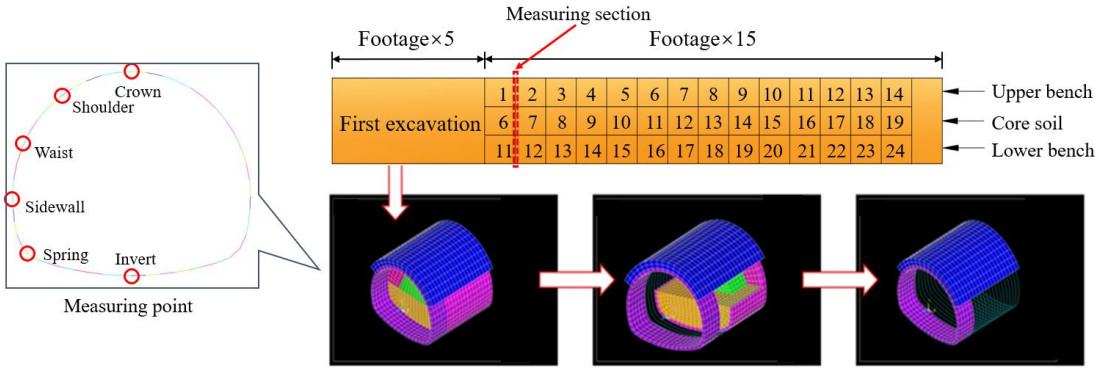

Fig. 6 Tunnel excavation process

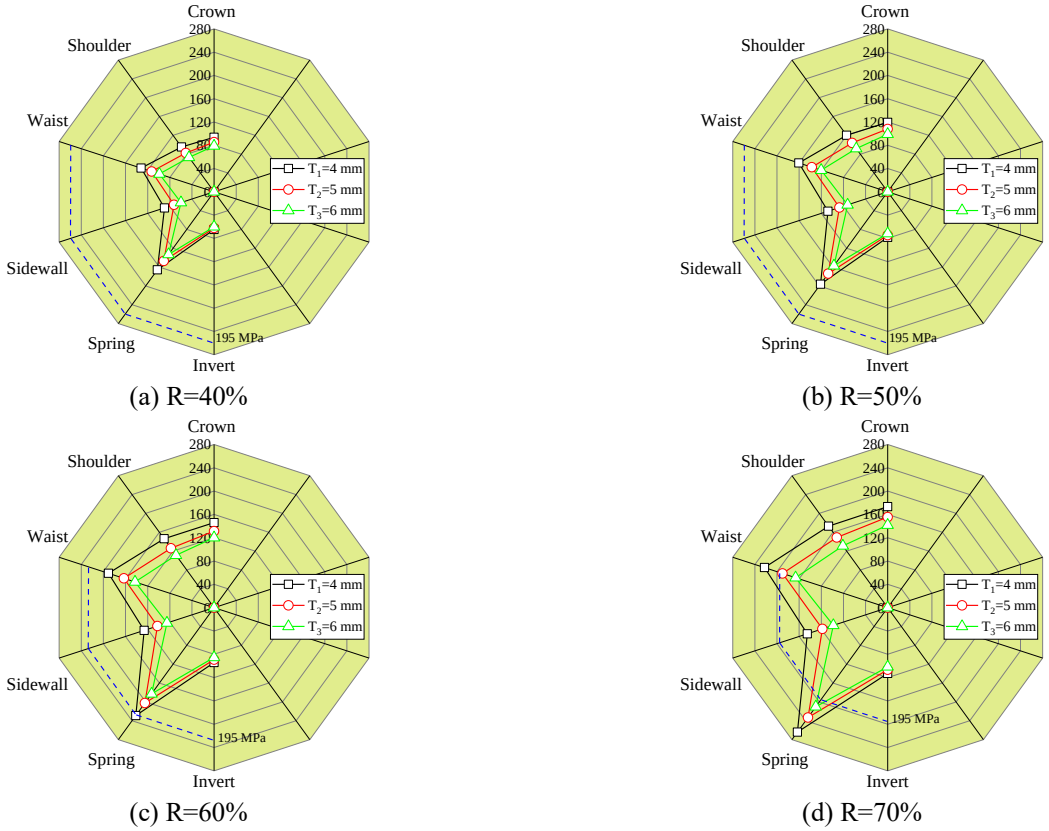

(a) R=40% (b) R=50%

(c) R=60% (d) R=70%

Fig. 7 Stress of arch under different thickness

process of gradual unloading of the ground that happens due to tunnel construction, as shown in Fig. 5 (Cui *et al.* 2015). In the actual engineering, there has a certain time interval between the construction procedures. To consider the space-time effect on the process of supporting, the calculation models for stress release conditions of the surrounding soil were assumed at R = 40%, R = 50%, R = 60%, and R = 70%, respectively (Fang *et al.* 2021, Vlachopoulos *et al.* 2009, Zhang *et al.* 2021a, Zheng *et al.* 2021).

The model surface was free to displace, while the model sides were constrained horizontally, and the model bottom was constrained vertically.

3.3 Construction scheme

Because the calculation model is symmetrical, only the left half was selected to define the characteristic points of the measurement control section (Ariznavarreta-Fernandez *et al.* 2016, Zhang *et al.* 2021b). The method of ring excavation that reserves core soil was used in the model. The excavation sequence and the measuring section are shown in Fig. 6. To eliminate the boundary effect, the middle section was as the target for measuring. The length of the first excavation was five times that of the excavation footage (full-section excavation), and the SCCS support was applied in the model. After that, the only support structure installed in each step was the π-shaped steel arch. Since the construction of the initial composite support system included three steps, a further 10% stress release was considered.

3.4 Instability assessment

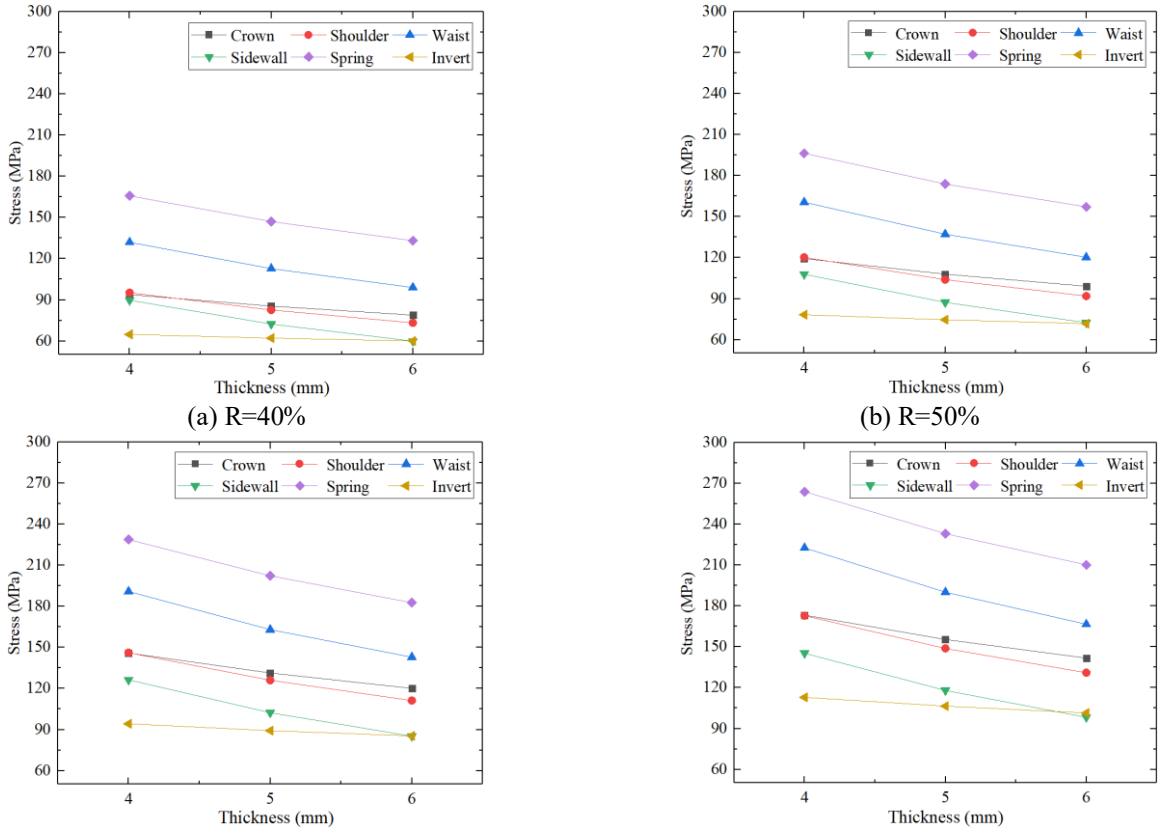

(a) R=40% (b) R=50%

(c) R=60% (d) R=70%

Fig. 8 Stress variation of arch under different thickness

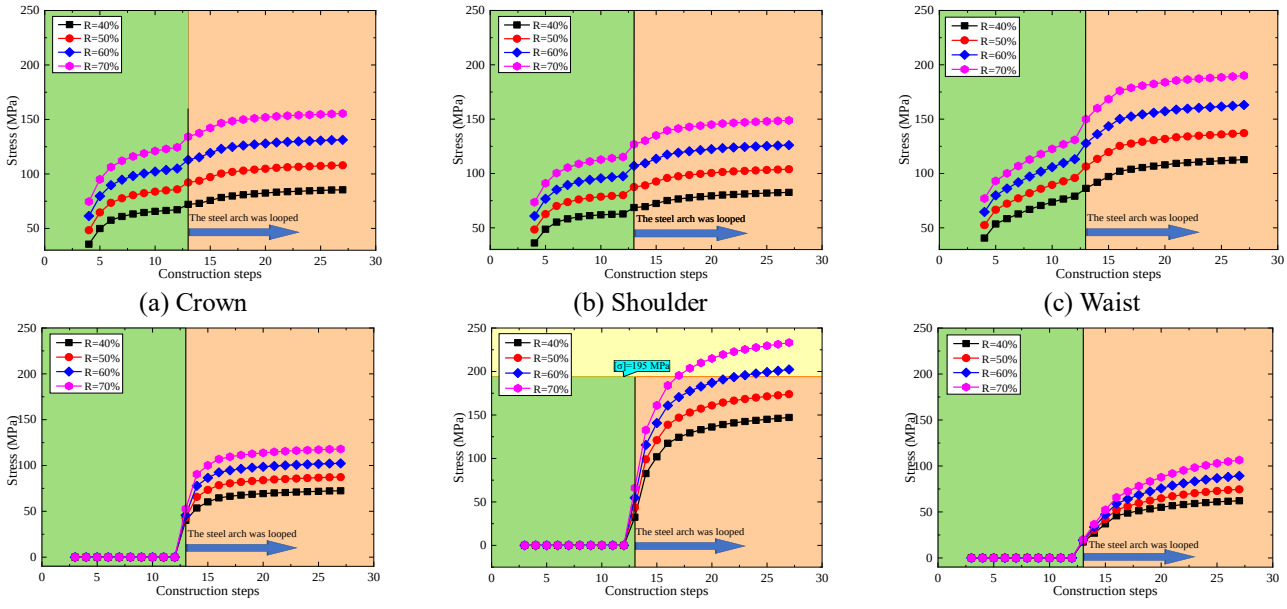

(a) Crown (b) Shoulder (c) Waist

(d) Sidewall (e) Spring (f) Invert

Fig. 9 Arch stress development under different stress release conditions

The steel material is considered structurally safe as long as the stress in the arch does not exceed 195 MPa (the allowable stress of Q235 steel). The maximum steel stress of the most relevant section of the steel arch was obtained from different excavation rounds to assess whether the π-shaped steel arch was damaged before grouting.

4. Results

4.1 Analysis of the steel arch thickness

The stress of the steel arches with varying wall thickness was calculated based on the stress release factors of the surrounding soil, as shown in Fig. 7. It can be seen that the

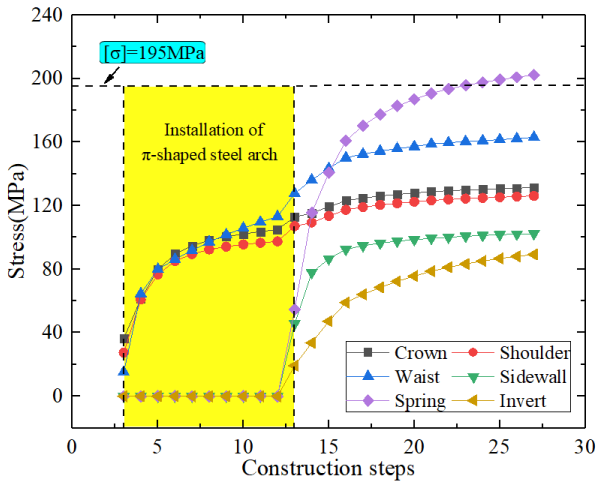

Fig. 10 The increasing process of π-shaped steel arch stress with excavation (T=5 mm, R=60%)

stress of the arch decreases with an increase in the thickness of the wall.

At a 40% stress release rate, the stress in the π-shaped steel arch at each key position was below the allowable maximum value, and the structure was safe. When the stress release rate of the surrounding soil was 50%, the stress in the arch at 5 mm and 6 mm of thickness was below the allowable maximum value, and the structure was safe. However, when the thickness of the arch decreased to 4 mm, the stress at the spring exceeded the allowable stress of steel, and the arch experienced plastic deformation. When the stress release rate of the surrounding soil reached 60%, the stress at each key position in the arch of a 6-mm thickness was below the allowable maximum value, and the structure was safe. Once the stress release rate of the surrounding soil reached 70%, the arch of any thickness experienced plastic deformation.

The influence of wall thickness on the stress of the arch is such that as the wall thickness increases, the stress decreases. Also, the maximum stress at the side wall and invert has a linearly decreasing trend; the maximum stress at the vault, arch shoulder, arch waist, and arch foot has a decreasing trend of a broken line, as shown in Fig. 8. When the wall thickness of an arch increases from 4 mm to 6 mm, the maximum stress reduction of the main dangerous section begins to go down, and the slope of the stress curve remains relatively gentle, which indicates that the benefits of structural safety caused by an increase in the wall thickness are gradually reduced. Therefore, the thickness of the arch wall is recommended to be 5 mm to avoid insufficient use of materials under the premise of ensuring safety.

4.2 Analysis of stress release rate

Fig. 9 shows the mechanical response of key positions of the π-shaped steel arch under different stress release rates when the wall thickness is 5 mm. It can be found that the stress of the arch increased linearly with an increase in the stress release rate. When the stress release rate of the surrounding soil was not higher than 50%, the grouting in the pipe could be completed within fourteen construction cycles after the arch was looped based on the construction conditions. When the stress release rate rose above 60%, the stress at the spring began to exceed the allowable stress of the steel. At that time, based on the construction conditions, the pipe grouting could be completed within eight construction cycles after the arch was looped. When the stress release rate of the surrounding soil reached 70%, the stress in the spring far exceeded the allowable level. Therefore, to ensure the safety of the π-shaped steel arch, the grouting in the pipe had to be completed within three construction cycles after the arch was looped. In summary, to ensure that the arch structure has a certain reserve of safety, as well as match the expectations of SCCS construction characteristics mentioned previously, it is necessary to reduce the release of stress in the surrounding soil using rapid and advanced support, and to keep it within 60%.

4.3 Structure stress development

Because stress variation in a π-shaped steel arch followed the same pattern at different wall thicknesses or under different stress release conditions, for sake of clarity, Fig. 10 demonstrates the stress evolution in an arch with a 5 mm wall thickness and a 60% rate of stress release.

With the upper bench advancing, the stress of the arch increased and tended to be flat. The stress of the arch clearly increased in the four footage. More specifically, the stresses at the arch at the crown, the shoulder, and the waist were close to each other, and the structure's dangerous zone was located at the waist. With the lower bench advancing, the stress of the arch showed a clear increase and then maintained a gentle stage. The stress of the arch clearly increased within the three footage of the lower bench advancing forward and then remained stable. At the same time, the stresses at the crown and shoulder of the arch were close to each other, increasing little, while the stress at the waist increased significantly and was greater than the stress at the crown or the shoulder.

When construction was completed, the stress at the arch's spring reached 202.35 MPa, exceeding the allowable value, while the other measuring points of the arch remained in the safe range. Therefore, grouting in the π-shaped steel arch should be completed within seven excavation footage after the arch is looped to ensure the safety of the structure. Because of the small arc radius and the expected stress concentration in the spring, some measures, such as bolting, should be taken to strengthen the area. In addition, it is very important to monitor the stress of the spring and the waist during construction.

4.4 Stress distribution of arch section

Compared to other common steel profiles, the cross-section size of the π-shaped steel arch is more complex, and it is unreasonable to simplify it as a structure with constant internal forces. Therefore, eight survey lines were established on the arch section (horizontal L1-L4, vertical L5-L8) to extract the nodal stresses on each survey line and analyze the stress distribution along the cross-section of the

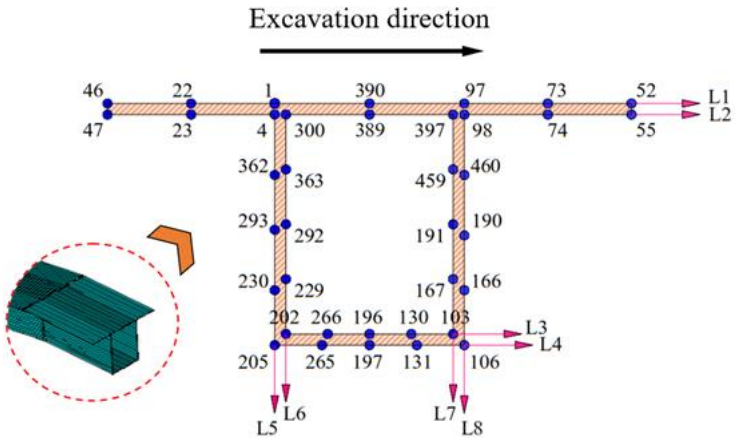

Fig. 11 Survey lines and nodes distribution of arch section

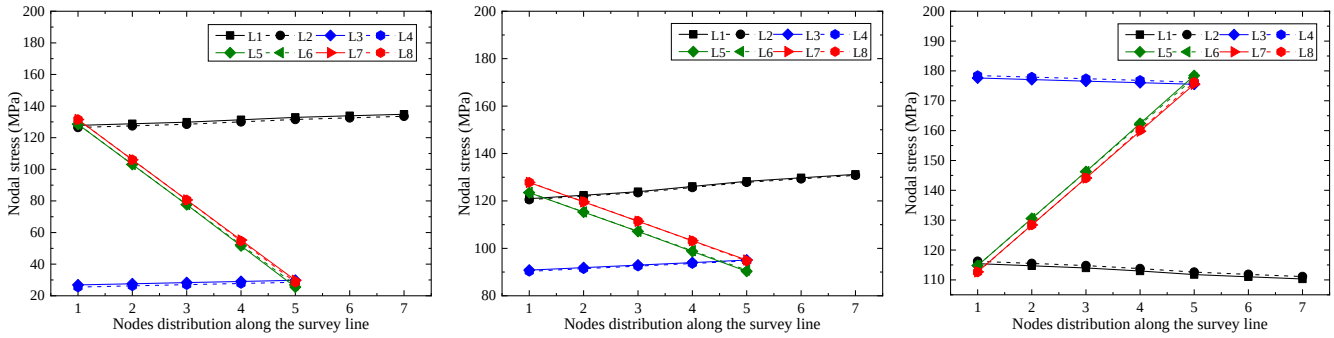

(a) Crown (b) Shoulder (c) Waist

Fig. 12 Stress distribution curves of the arch section

steel arch, as shown in Fig. 11.

The stress distribution curves of the arch section at key positions were drawn based on the calculation of a 5 mm wall thickness and a 60% stress release rate, as shown in Fig. 12. Because the ring cut method with conservation of core soil was adopted, so the upper bench arch has the most concerned. The stress distribution characteristics of the crown and the shoulder were as follows:

(1) Along the horizontal direction of the section, the nodes stresses of the L1, L2, L3, and L4 survey lines gradually increased along the excavation direction, indicating that the stress was greater on the wing closer to the tunnel face.

(2) Along the vertical direction of the section, the nodes stress of the L5, L6, L7, and L8 survey lines decreased gradually along the survey line direction, which indicates that the arch section closes to the surrounding soil had higher stress due to the downward surrounding soil pressure.

The stress distribution at the waist was opposite to that at the crown and the shoulder (see Fig. 12(c)). There are two main reasons for this difference:

(1) The waist was in the resistance area, and the closer it was to the tunnel face, the greater was the elastic resistance provided by the surrounding soil.

(2) The emergence of the reverse bending point made the bending moment at the waist change from positive to negative, which increased the compressive stress of the arch sections located further away from the surrounding soil.

5. Discussion

5.1 Optimization of the installation gap

5.1.1 Model description

The following section considers a 3D model with a 5 mm wall thickness and a 60% stress release rate of the surrounding soil, with the installation gap of the arch being set at 0 cm, 2.5 cm, 5 cm, 7.5 cm, and 10 cm, respectively, as shown in Fig. 13.

5.1.2 Structural stress characteristics

Fig. 14 shows the development of the overall stress of the arch with the change in the installation gap. The stress of the arch at key positions increases linearly with an increase in the installation gap. Except for the spring, the stress of other parts of the arch remains in a safe range. When the installation gap is increased from 0 cm to 10 cm, the stress at the crown, shoulder, and waist is increased by 5.83 MPa, 7.95 MPa, and 8.40 MPa, respectively, with the stress growth rate reaching 4.4%, 6.3%, and 5.2%, respectively. Therefore, the arch's installation gap within 10 cm has little effect on the stress of the whole structure. It should be pointed out, however, since the calculation did not consider the fall of the soil mass, it was necessary to increase the installation gap of the arch based on the actual surrounding soil conditions to ensure that the soil mass did not fall.

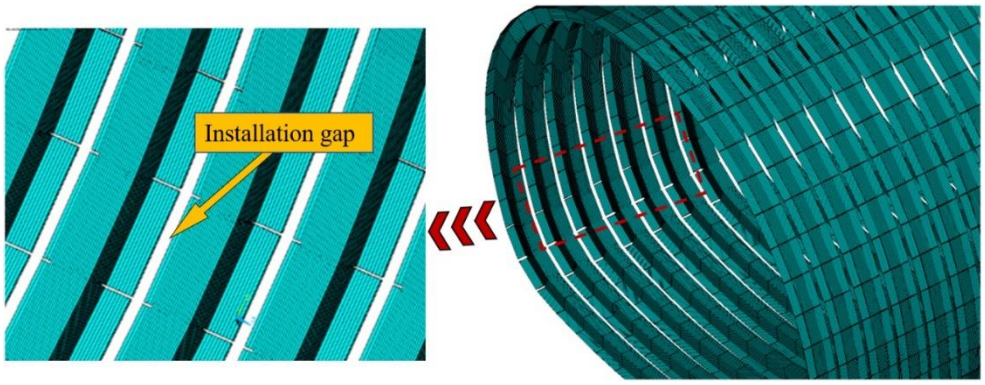

Fig. 13 Installation gap of π-shaped steel arch

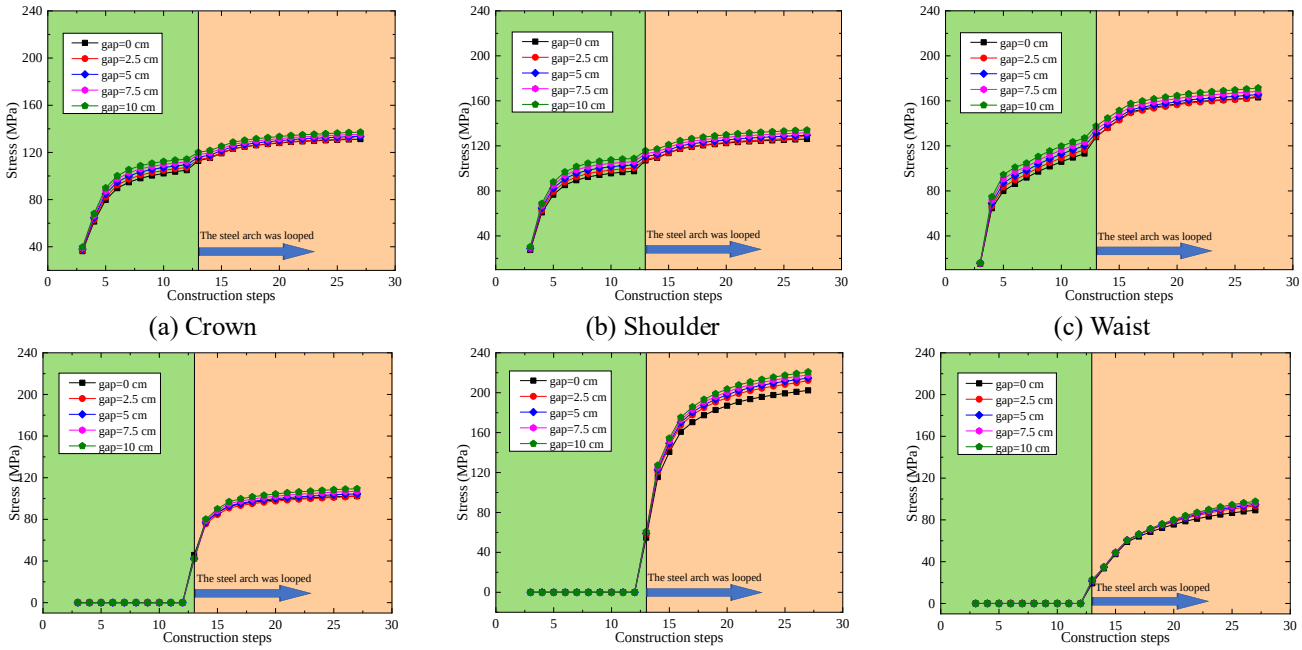

(a) Crown (b) Shoulder (c) Waist

(d) Sidewall (e) Spring (f) Invert

Fig. 14 Arch stress development under different installation gaps

5.1.3 Sectional stress characteristics

Because the method of ring excavation that reserves core soil was adopted, so the upper bench arch has the most concerned. It can be seen from the previous calculation results that the maximum stress survey lines at the crown, shoulder, and waist of the arch were L1, L1, and L4 respectively. The equivalent stress of the nodes on these survey lines was extracted, and the stress curves of the arch section under different installation gaps were drawn, as shown in Fig. 15.

With an increase in the installation gap of the π-shaped steel arch section, the node stress at the crown and shoulder showed a "steps" growth trend (2.5 cm < gap ≤ 5 cm was the platform stage), and the node stress at the waist showed a two-stage growth trend (gap ≤ 5 cm was the slow growth stage, and 5 cm < gap ≤ 10 cm was the fast growth stage). Therefore, it was determined that the installation gap of the π-shaped steel arch should be 5 cm.

5.2 Comparative analysis of different support systems

5.2.1 Model description

The excavation models of the loess tunnel with the traditional support structure and the SCCS were established respectively. The traditional support system included an I20b steel arch and C30 concrete (the thickness of the initial support and the secondary lining was 26 cm and 50 cm, respectively). As a contrast, the SCCS included a π-shaped steel arch (installation gap of 5 cm and a wall thickness of 5 mm) and C30 concrete (the thickness of sealing concrete and secondary lining was 40 cm and 30 cm, respectively). The material parameters of an I20b steel arch and a π-shaped steel arch were the same, and the other parameters used in the calculation are listed in Table 1.

The horizontal calculation range of the model was three times the tunnel diameter (3D), the bottom calculation range was four times the tunnel diameter (4D), and the longitudinal length was 30 m. To reduce the influence of the boundary effect, the model adopted a three-stage excavation, with the excavation footage of 0.75 m. The excavation method is shown in Fig. 16.

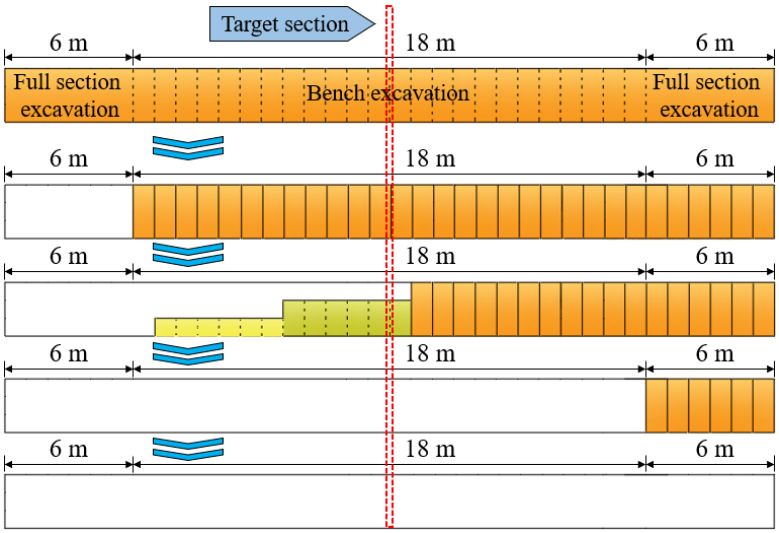

Fig. 16 Sequential excavation method with core soil

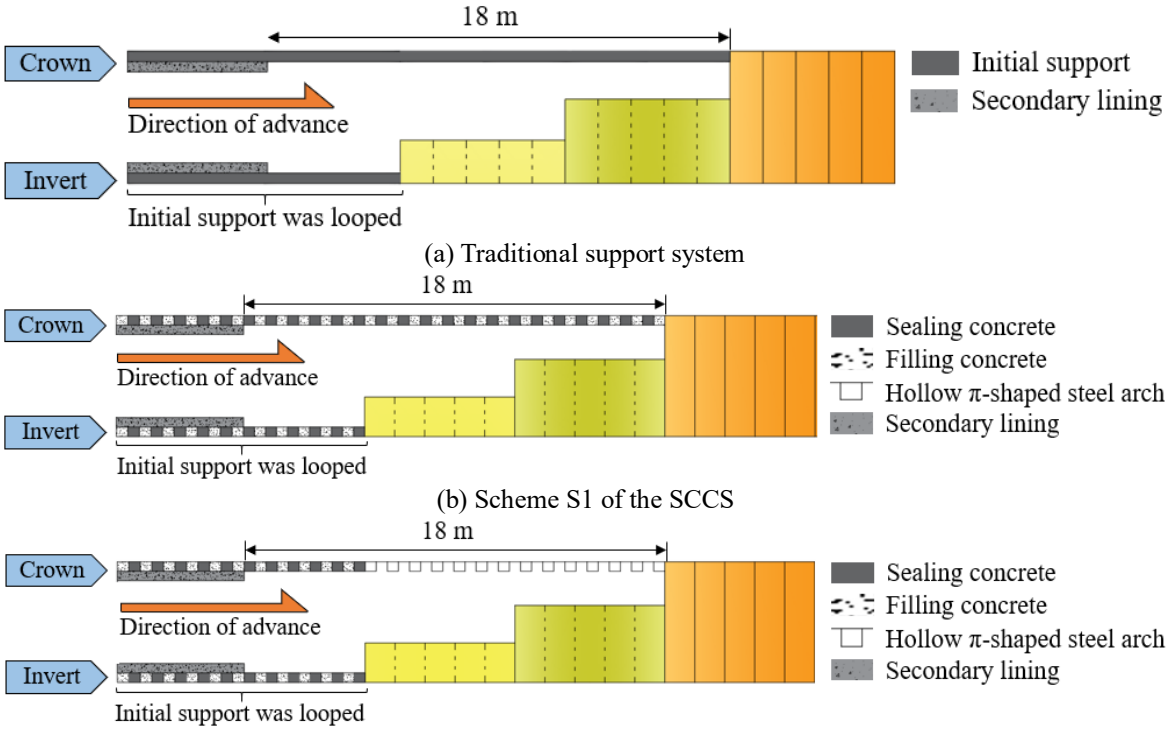

(a) Traditional support system

(b) Scheme S1 of the SCCS

(c) Scheme S2 of the SCCS

Fig. 17 Comparison of support schemes

To reflect the flexibility of the SCCS, two totally different construction schemes were established, as represented by S1 and S2 shown in Fig. 17.

5.2.2 Deformation analysis

Using the middle section (L = 15 m) (shown in Fig. 16) as a target, Fig. 18 presents the settlement of the crown throughout the whole construction process. The process went through the following five development stages: (1) The early stage, in which the settlement occurred before the excavation of the target section and accounted for only about 12% of the total settlement. (2) The rapid development stage, in which the settlement occurred during the excavation of the target section, and the support structure was not looped. During this stage the settlement clearly increased, accounting for 78% of the total settlement. (3) The gentle development stage, in which the settlement increased gently after the support structure in the target section was looped. (4) The saltatorial stage, in which the excavation affected the target section due to the three-stage excavation of the model, and the increased settlement accounted for about 5% of the total settlement. (5) The stability stage, in which the settlement occurred after the tunnel was completed. The settlement remained basically stable, though the installation of the secondary lining caused a small growth of the settlement. The excavation and

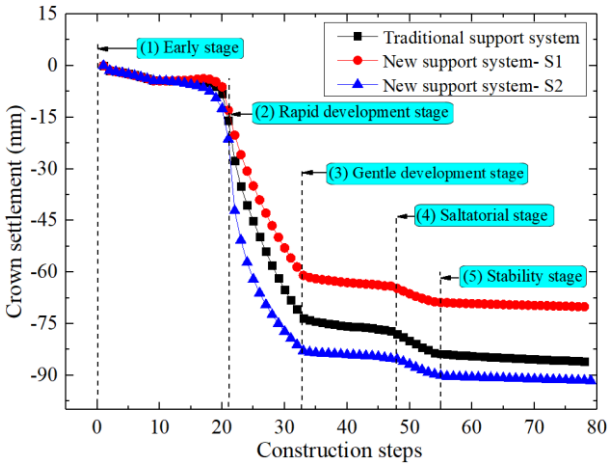

Fig. 18 Crown settlement curve

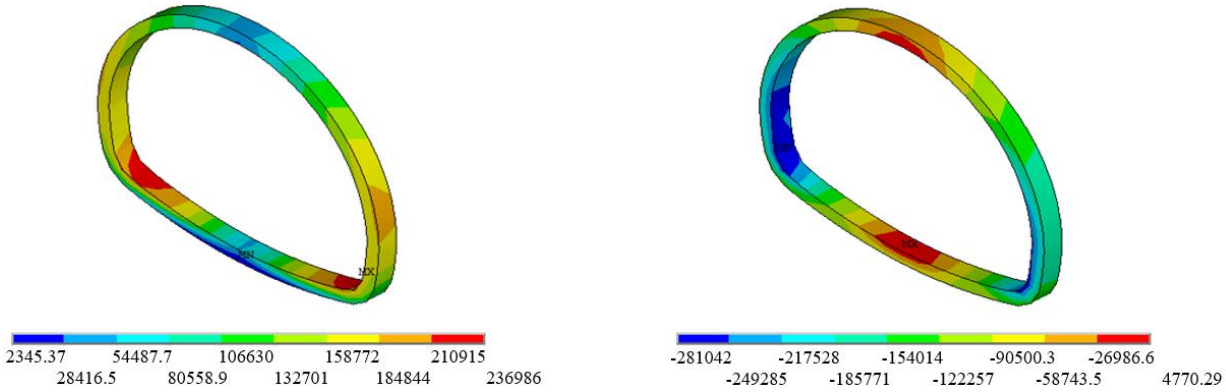

(a) First principal stress (b) Third principal stress

Fig. 19 The secondary lining stress of traditional support system

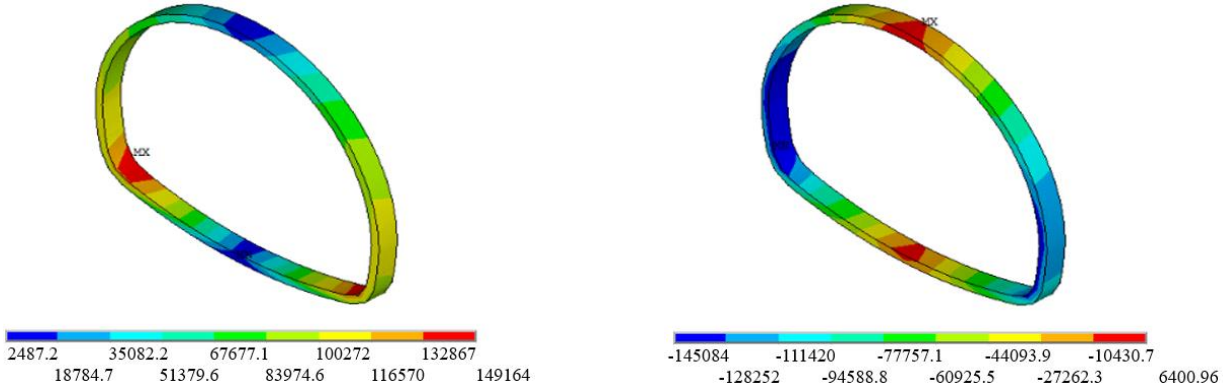

(a) First principal stress (b) Third principal stress

Fig. 20 The secondary lining stress of the SCCS (S1)

support process of the target section had a significant impact on the overall settlement, indicating that it is necessary to improve the initial strength of the support in a loess tunnel.

Compared to a conventional support structure, the settlement of the S1 scheme was reduced by 15.88 mm. However, the settlement of the S2 scheme was increased by 5.56 mm. It can be found that if the construction sequence of the SCCS is consistent with the conventional support system, the settlement is significantly improved under the same construction rate of progress. In addition, if the construction sequence of the SCCS is simplified, and the excavation of the face is completed only with a π-shaped steel arch support, the settlement is slightly increased while the construction time can be greatly reduced. To strike a balance between settlement control and construction speed, the full-section sealing concrete of SCCS could be optimized as a half-section construction, which represents the upper and lower bench are constructed respectively for the sealing concrete installation.

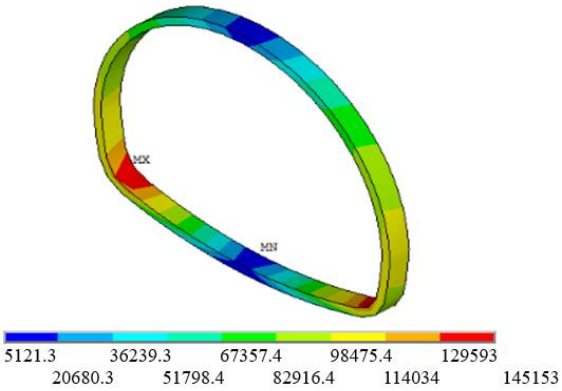

(a) First principal stress

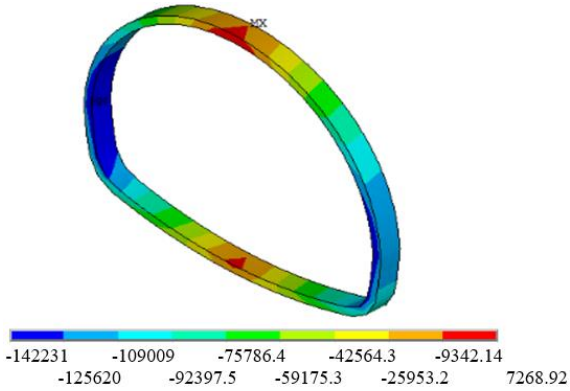

(b) Third principal stress

Fig. 21 The secondary lining stress of the SCCS (S2)

5.2.3 Stress contrast of secondary lining

As a permanent support structure, the secondary lining bears the load transmitted by the initial support. Its stress state not only determines the safety of the tunnel, but also reflects the safety margin of the structure.

Figs. 19 to 21 show the secondary lining stress of the target section under different support systems. The maximum tensile stress appears on the inner side of the spring, and the maximum compressive stress appears on the inner side of the sidewall.

The maximum values of the first principal stress and the third principal stress of the traditional support system are 0.237 MPa and 0.281 MPa, respectively. The maximum values of the first principal stress of the composite structure support system are 0.149 MPa (S1) and 0.145 MPa (S2), and the maximum values of the third principal stress are 0.145 MPa (S1) and 0.142 MPa (S2). Due to the "early strength" characteristics of the SCCS, the maximum tensile and compressive stresses of the secondary lining in the S1 scheme are reduced by 0.088 MPa and 0.136 MPa, respectively, with the reduction rates of 37.1% and 48.4%. The maximum tensile and compressive stresses of the secondary lining in the S2 scheme are reduced by 0.092 MPa and 0.139 MPa, respectively, with a reduction rate of 38.8% and 49.5%, respectively. Additionally, due to the larger stress release rate of the surroundings in the S2 scheme, the secondary lining has the least amount of stress.

6. Conclusions

This paper reflected on the current issues of traditional support for the tunnels constructed in loess and proposed a novel support system named Steel-Concrete Composite Support System (SCCS) based on the principles of primary lining reinforcement and rapid construction. The system was studied via a three-dimensional numerical model by using ANSYS 19.0 to obtain the support characteristics of SCCS during tunneling. The support parameters and construction performance were also investigated. The conclusions and suggestions are as follows:

• To ensure the safety of a π-shaped steel arch and make full use of the supporting performance, the wall thickness is recommended to be 5 mm.

• To maintain the safety reserve of the arch structure, it is necessary to control the stress release rate within 60%.

• In the horizontal direction of the arch section, the node stress at the crown and shoulder gradually increased along the excavation direction. In the vertical direction, the node stress gradually decreased from top to bottom. Contrarily, the stress distribution at the waist were completely opposite to that at the crown and shoulder.

• With an increase in the installation gap of the π-shaped steel arch section, the node stress at the crown and shoulder showed a stepped growth trend, which was barely growing in the range of 2.5 cm to 5 cm. Comparatively, the node stress that of at the waist showed accelerated growth when the installation gap was greater than 5 cm.

• Compared to the traditional support system, SCCS provided better control of the deformation of the surrounding soil. The maximum tensile and compressive stresses of the secondary lining were on average reduced by 38.0% and 49.0%, respectively.

Acknowledgments

This study was supported by the National Natural Science Foundation of China (Grant No. 52008028, 52078421) and the Fundamental Research Funds for the Central Universities, CHD (Grant No. 300102210112).

References

Al Zand, A.W., Badaruzzaman, W.H.W., Mutalib, A.A. and Hilo, S.J. (2016), "The enhanced performance of CFST beams using different strengthening schemes involving unidirectional CFRP sheets: An experimental study", *Eng. Struct.*, **128**, 184-198. https://doi.org/10.1016/j.engstruct.2016.09.044.

Ariznavarreta-Fernandez, F., Gonzalez-Palacio, C., Menendez-Diaz, A. and Ordonez, C. (2016), "Measurement system with angular encoders for continuous monitoring of tunnel convergence", *Tunn. Undergr. Sp. Tech.*, **56**, 176-185. https://doi.org/10.1016/j.tust.2016.03.014.

Bjureland, W., Spross, J., Johansson F., Prastings, A. and Larsson, S. (2017), "Reliability aspects of rock tunnel design with the observational method", *Int. J. Rock Mech. Min. Sci.*, **98**, 102-110. https://doi.org/10.1016/j.ijrmms.2017.07.004.

Bonini, M., Lancellotta, G. and Barla, G. (2013), "State of stress in tunnel lining in squeezing rock conditions", *Rock Mech. Rock Eng.*, **46**(2), 405-411. https://doi.org/10.1007/s00603-012-0326-y.

Chang, X., Luo, X.L., Zhu, C.X. and Tang, C.N. (2014), "Analysis of circular concrete-filled steel tube (CFT) support in high ground stress conditions", *Tunn. Undergr. Sp. Tech.*, **43**, 41-48. https://doi.org/10.1016/j.tust.2014.04.002.

Chen, J.X., Xu, Z.L., Luo, Y.B., Song, J.K., Liu, W.W. and Dong, F.F. (2020), "Application of the upper-bench CD method in super large-span and shallow tunnel: A case study of Letuan Tunnel", *Adv. Civ. Eng.* https://doi.org/10.1155/2020/8826232.

Cui, L., Zheng, J.J., Zhang, R.J. and Lai, H.J. (2015), "A numerical procedure for the fictitious support pressure in the application of the convergence-confinement method for circular tunnel design", *Int. J. Rock Mech. Min. Sci.*, **78**, 336-349. https://doi.org/10.1016/j.ijrmms.2015.07.001.

Dancygier, A.N., Karinski, Y.S. and Chacha, A. (2016), "A model to assess the response of an arched roof of a lined tunnel", *Tunn. Undergr. Sp. Tech.*, **56**, 211-225. https://doi.org/10.1016/j.tust.2016.03.009.

Doostmohammadi R. (2016), "Investigation of swelling pressure of weak rocks in vicinity of support systems", *J. Min. Sci.*, **52**(3), 473-480. https://doi.org/10.1134/S1062739116030670.

Fang, Q., Du, J.M., Li, J.Y., Zhang, D.L. and Cao, L.Q. (2021), "Settlement characteristics of large-diameter shield excavation below existing subway in close vicinity", *J. Cent. South Univ.*, In Press.

GB 50936-2014 (2014), Technical Code for Concrete Filled Steel Tubular Structures, Ministry of Housing and Urban-Rural Development of the People's Republic of China, Beijing, China.

Hassanein, M.F., Patel, V.I., El Hadidy, A.M., Al Abadi, H. and Elchalakani, M. (2018), "Structural behaviour and design of elliptical high-strength concrete-filled steel tubular short compression members", *Eng. Struct.*, **173**, 495-511. https://doi.org/10.1016/j.engstruct.2018.07.023.

He, S.Y., Lai, J.X. and Zhong, Y.J. (2021), "Damage behaviors, prediction methods and prevention methods of rockburst in 13 deep traffic tunnels in China", *Eng. Fail. Anal.*, **121**, 105178. https://doi.org/10.1016/j.engfailanal.2020.105178.

Hua, J.X. (2018), *Geological Engineering Handbook*, China Architecture & Building Press, Beijing, China.

Huang, W.P., Yuan, Q., Tan, Y.L., Wang, J., Liu, G.L., Qu, G.L. and Li, C. (2018), "An innovative support technology employing a concrete-filled steel tubular structure for a 1000-m-deep roadway in a high in situ stress field", *Tunn. Undergr. Sp. Tech.*, **73**, 26-36. https://doi.org/10.1016/j.tust.2017.11.007.

JTG 3370.1-2018 (2018), Specifications for design of highway tunnels, Ministry of Transport of the People's Republic of China, Beijing, China.

Kaya, A., Karaman, K. and Bulut, F. (2017), "Geotechnical investigations and remediation design for failure of tunnel portal section: A case study in northern Turkey", *J. Mountain Sci.*, **14**(6), 1140-1160. https://doi.org/10.1007/s11629-016-4267-x.

Khan, U.H., Mitri, H.S. and Jones, D. (1996), "Full scale testing of steel arch tunnel supports", *Int. J. Rock Mech. Min. Sci.*, **33**(3), 219-232. https://doi.org/10.1016/0148-9062(95)00065-8.

Lai, H.P., Song, W.L. and Liu, Y.Y. (2017), "Influence of flooded loessial overburden on the tunnel lining: Case study", *J. Perform. Constr. Fac.*, **31**(6), 04017108. https://doi.org/10.1061/(ASCE)CF.1943-5509.0001100.

Li, H., Ma, E.L., Lai, J.X., Wang, L.X., Xu, S.S., Wang, K. and Liu T. (2020), "Tunnelling-induced settlement and treatment techniques for a Loess Metro in Xi'an", *Adv. Civ. Eng.* https://doi.org/10.1155/2020/1854813.

Li, S.C., Lu, W., Wang, Q. and Sun, H.B., Jiang, B. and Qin, Q. (2018), "Study on failure mechanism and mechanical properties of casing joints of square steel confined concrete arch", *Eng. Fail. Anal.*, **92**, 539-552. https://doi.org/10.1016/j.engfailanal.2018.05.011.

Li, W.T., Yang, N., Mei, Y.C., Zhang, Y.H., Wang, L. and Ma, H.Y. (2020), "Experimental investigation of the compression-bending property of the casing joints in a concrete filled steel tubular supporting arch for tunnel engineering", *Tunn. Undergr. Sp. Tech.*, **96**, 103184. https://doi.org/10.1016/j.tust.2019.103184.

Liu, K.Q., Li, S.C., Ding, W.T., Hou, M.L., Gong, Y.J. and Li, H.L. (2020a), "Pre-supporting mechanism and supporting scheme design for advanced small pipes in the silty clay layer", *Tunn. Undergr. Sp. Tech.*, **98**, 103259. https://doi.org/10.1016/j.tust.2019.103259.

Liu, T., Xie, Y., Feng, Z.H., Luo, Y.B., Wang, K. and Xu, W. (2020b), "Better understanding the failure modes of tunnels excavated in the boulder-cobble mixed strata by distinct element method", *Eng. Fail. Anal.*, **116**, 104712. https://doi.org/10.1016/j.engfailanal.2020.104712.

Liu, Y.Y. and Lai, H.P. (2019), "Load characteristics of tunnel lining in flooded loess strata considering loess structure", *Adv. Civ. Eng.* https://doi.org/10.1155/2019/3731965.

Liu, Y.Y., Lai, H.P., Xie, Y.L. and Song, W.L. (2017), "Cracks analysis of highway tunnel lining in flooded loess", *P. I. Civ. Eng. Geotech.*, **170**(1), 62-72. https://doi.org/10.1680/jgeen.15.00177.

Liu, X.G., Zhang, W.P., Gu, X.L. and Ye, Z.W. (2021). "Probability distribution model of stress impact factor for corrosion pits of high-strength prestressing wires", *Eng Struct.*, **230**. https://doi.org/10.1016/j.engstruct.2020.111686.

Liu, Z.D. (1997), *Mechanics and Engineering of Loess*, Shanxi Science and Technology Press, Xi'an, China.

Mao, Z.J., Wang, X.K., An, N., Li, X.J. and Wei, R.Y. (2019), "Water disaster susceptible areas in loess multi-arch tunnel construction under the lateral recharge condition", *KSCE J. Civ. Eng.*, **23**(10), 4564-4577. https://doi.org/10.1007/s12205-019-0951-z.

Ozdogan, M.V., Yenice, H., Gonen, A. and Karakus, D. (2018), "Optimal support spacing for steel sets: Omerler underground coal mine in Western Turkey", *Int. J. Geomech.*, **18**(2), 05017003. https://doi.org/10.1061/(ASCE)GM.1943-5622.0001069.

Prazeres, P.G.C., Thoeni, K. and Beer, G. (2012), "Nonlinear analysis of NATM tunnel construction with the boundary element method", *Comput. Geotech.*, **40**, 160-173. https://doi.org/10.1016/j.compgeo.2011.10.005.

Rahimi, B., Shahriar, K. and Sharifzadeh, M. (2014), "Evaluation of rock mass engineering geological properties using statistical analysis and selecting proper tunnel design approach in Qazvin-Rasht railway tunnel", *Tunn. Undergr. Sp. Tech.*, **41**, 206-222. https://doi.org/10.1016/j.tust.2013.12.010.

Rehman, H., Ali W., Naji A.M., Kim, J.J., Abdullah, R.A. and Yoo, H.K. (2018), "Review of rock-mass rating and tunneling quality index systems for tunnel design: Development, refinement, application and limitation", *Appl. Sci.*, **8**(8), 1250. https://doi.org/10.3390/app8081250.

Skrzypkowski, K., Korzeniowski, W., Zagorski, K. and Zagorska, A. (2019), "Flexibility and load-bearing capacity of roof bolting as functions of mounting depth and hole diameter", *Energies*, **12**(19), 3754 https://doi.org/10.3390/en12193754.

Song, W.L., Lai, H.P., Liu, Y.Y., Yang, W.H. and Zhu, Z.D. (2019), "Field and laboratory study of cracking and safety of secondary lining for an existing highway tunnel in loess ground", *Tunn. Undergr. Sp. Tech.*, **88**, 35-46. https://doi.org/10.1016/j.tust.2019.02.018.

Vlachopoulos, N. and Diederichs, M.S. (2009), "Improved longitudinal displacement profiles for convergence confinement analysis of deep tunnels", *Rock Mech. Rock Eng.*, **42**(2), 131-

146. https://doi.org/10.1007/s00603-009-0176-4.
Wang, H.T., Li, S.C., Wang, Q., Wang, D.C., Li, W.T., Liu, P., Li, X.J. and Chen, Y.J. (2019a) "Investigating the supporting effect of rock bolts in varying anchoring methods in a tunnel", *Geomech. Eng.*, **19**(6), 485-498. https://doi.org/10.12989/gae.2019.19.6.485.
Wang, Q., Jiang, B., Li, Y., Shao, X., Wang, F.Q., Li, S.C., Zhang, S.G. and Ruan, G.Q. (2017), "Mechanical behaviors analysis on a square-steel-confined-concrete arch centering and its engineering application in a mining project", *Eur. J. Environ. Civ. Eng.*, **21**(4), 389-411. https://doi.org/10.1080/19648189.2015.1124809.
Wang, Q., Luan, Y.C., Jiang, B., Li, S.C., He, M.C., Sun, H.B., Qin, Q. and Lu, W. (2019b), "Study on key technology of tunnel fabricated arch and its mechanical mechanism in the mechanized construction", *Tunn. Undergr. Sp. Tech.*, **83**, 187-194. https://doi.org/10.1016/j.tust.2018.10.002.
Wang, Z.C. (2019), "Analysis on characteristics of composite structure support system in loess tunnel", Ph.D. Thesis, Highway School, Chang'an University, Xi'an, China.
Wang, Z.C., Du, K., Xie, Y.L., Su, X.L., Shi, Y.F., Li, X. and Liu, T. (2021a), "Buckling analysis of an innovative type of steel-concrete composite support in tunnels", *J. Construct. Steel Res.*, **179**, 106503. https://doi.org/10.1016/j.jcsr.2020.106503.
Wang, Z.C., Shi; Y.F., Xie; Y.L., Zhang, M.Z., Liu, T. and Li, C. (2021b), "Support characteristic of a novel type of support in loess tunnels using the convergence-confinement method", *Int. J. Geomech.*, In Press.
Wang, Z.C., Su, X.L., Lai, H.P., Xie, Y.L., Qin, Y.W. and Liu, T. (2021c), "Conception and evaluation of a novel type of support in loess tunnels", *J. Perform. Constr. Fac.*, **35**(1), 04020144. https://doi.org/10.1061/(ASCE)CF.1943-5509.0001533.
Wang, Z.C., Xie, Y.L., Liu, H.Q. and Feng, Z.H. (2021d), "Analysis on deformation and structural safety of a novel concrete-filled steel tube support system in loess tunnel", *Eur. J. Environ. Civ. Eng.*, **25**(1), 39-59. https://doi.org/10.1080/19648189.2018.1515665.
Wu, H., Zhong, Y.J., Xu, W., Shi, W.S.Y., Shi, X.H. and Liu, T. (2020), "Experimental investigation of ground and air temperature fields of a cold-region road tunnel in NW China", *Adv. Civ. Eng.* https://doi.org/10.1155/2020/4732490.
Wu, K., Shao, Z., Qin, S., Wei, W. and Chu, Z. (2021), "A critical review on the performance of yielding supports in squeezing tunnels", *Tunn. Undergr. Sp. Tech.*, **114**(1). https://doi.org/10.1016/j.tust.2021.103815.
Xue, Y.G., Zhang, X.L., Li, S.C., Qiu, D.H., Su, M.X., Xu, Z.H., Zhou, B.H. and Xia, T. (2019), "Sensitivity analysis of loess stability to physical and mechanical properties: Assessment model", *Int. J. Geomech.*, **19**(7), 06019012. https://doi.org/10.1061/(ASCE)GM.1943-5622.0001400.
Yoo, C. and Choi, J. (2018), "Effect of construction sequence on three-arch tunnel behavior-Numerical investigation", *Geomech. Eng.*, **15**(3), 911-917. https://doi.org/10.12989/gae.2018.15.3.911.
Zhang, J.C., Yan, Q.X., Sun, M.H., Li, B.J., Chen, W.Y. and Chen, H. (2021a), "Experimental study on the vibration damping of two parallel shield tunnels connected by an assembled transverse passage", *Tunn. Undergr. Sp. Tech.*, **107**, 103659. https://doi.org/10.1016/j.tust.2020.103659.
Zhang, W.J., Li, W.T., Yang, N., Wang, Q., Li, T.C. and Wang, G. (2017), "Determination of the bearing capacity of a concrete-filled steel tubular arch support for tunnel engineering: Experimental and theoretical studies", *KSCE J. Civ. Eng.*, **21**(7), 2932-2945. https://doi.org/10.1007/s12205-017-1418-8.
Zhang, Y.J., Su, K., Qian, Z.D. and Wu, H.G. (2019a), "Improved longitudinal displacement profile and initial support for tunnel excavation", *KSCE J. Civ. Eng.*, **23**(6), 2746-2755. https://doi.org/10.1007/s12205-019-0411-9.
Zhang, Y.W., Weng, X.L., Song, Z.P. and Sun, Y.F. (2019b), "Modeling of loess soaking induced impacts on a metro tunnel using a water soaking system in centrifuge", *Geofluids*. https://doi.org/10.1155/2019/5487952.
Zhang, Y.W., Yang, T. and Liu, T. (2021b), "Seismic performance of mortise-groove prefabricated metro station based on dynamic constitutive model", *Shock Vib.* https://doi.org/10.1155/2021/8873212.
Zhang, Z.P., Zhou, Z.J., Guo, T., Xu, T.Y. and Zhu, L.X. (2021c), "A measuring method for layered compactness of loess subgrade based on hydraulic compaction", *Meas. Sci. Technol.*, **32**(4).
Zheng, H.B., Li, P.F., Ma, G.W. (2021), "Stability analysis of the middle soil pillar for asymmetric parallel tunnels by using model testing and numerical simulations", *Tunn. Undergr. Sp. Tech.*, **108**, 103686. https://doi.org/10.1016/j.tust.2020.103686
Zhou, S.H., Tian, Z.Y., Di, H.G., Guo, P.J. and Fu, L.L. (2020), "Investigation of a loess-mudstone landslide and the induced structural damage in a high-speed railway tunnel", *B. Eng. Geol. Environ.*, **79**(5), 2201-2212. https://doi.org/10.1007/s10064-019-01711-y.
Zhu, Y.M., Chen, L., Zhang, H., Zhou, Z.L. and Chen, S.G. (2019), "Physical and mechanical characteristics of soft rock tunnel and the effect of excavation on supporting structure", *Appl. Sci.*, **9**(8), 1517. https://doi.org/10.3390/app9081517.

CC